# High optical absorber of $WS_2/MoS_2$ Si-based in broadband spectrum

XICHENG XIONG[1,*], CHUN JIANG[2], QUAN XIE[3], QUANZHEN HUANG[1], XINGHUI WU[1], YUBI ZHANG[1]
[1]*School of Electrical and Information Engineering, Henan University of Engineering, Zhengzhou 451191, China*
[2]*State Key Laboratory of Advanced Optical Communication Systems and Networks, Shanghai Jiao Tong University, Shanghai 200240, China*
[3]*School of Big Data and Information Engineering, Guizhou University, Guiyang 550025, China*

In this paper, the authors present the design of three distinct simple structures: Si, $MoS_2$/Si, and $WS_2/MoS_2$/Si film. The objective is to analyze their optical transmission properties across a broadband range. The findings reveal that the absorptivity of $WS_2/MoS_2$/Si was exceptional, exhibiting an expanded band range and increased value. These results suggest that this structure holds great potential for application in various photodevices. Such characteristics are highly advantageous for the design and fabrication of optical and photoelectric devices.

(Received October 28, 2024; accepted August 5, 2025)

*Keywords*: $WS_2$, $MoS_2$, Si, Optical property, Absorber

## 1. Introduction

In recent decades, transition metal dichalcogenides (TMDCs) have emerged as promising materials with a wide range of applications. They have garnered extensive research attention, particularly in the fields of nanoelectronics and photonics [1, 2]. Among TMDCs, $MoS_2$ and $WS_2$ have gained significant interest due to their high absorption coefficient [1, 2]. On the other hand, silicon (Si) is a widely used semiconductor material in various electronic and photoelectric devices. Its excellent physical properties have made it a staple in modern society [3-6]. In fact, nearly all modern semiconductor devices, including integrated circuits and photodetectors, are fabricated on silicon substrates. Combining the properties of $MoS_2$, $WS_2$, and Si, these materials can be applied together in photodetectors [7-10].

The photodetector must be constructed using a material or structure with high optical absorption. Materials such as $MoS_2$, $WS_2$, and Si exhibit greater optical absorption. $MoS_2$ and $WS_2$ are classified as two-dimensional materials. Single-layer $MoS_2$ has a direct bandgap of 1.8 eV, and the bandgap of $MoS_2$ can be adjusted by altering the number of layers in the crystal [11, 12]. The lattice constants for $WS_2$ and $MoS_2$ crystals are 0.315 nm and 0.312 nm, respectively [12]. Monolayer $WS_2$ is also a direct band material with a value of 1.50 eV due to quantum confinement. The number of layers or their thickness can impact the optical refractive index and physical performance of these materials. Bulk and multilayer $MoS_2$ and $WS_2$ are considered indirect gap materials [13]. Additionally, $MoS_2$ and $WS_2$ possess low surface energy, and the energy of the $WS_2/MoS_2$ heterostructure is approximately 1.96 eV [12]. These characteristics broaden their potential applications in semiconductor and optoelectrical devices. However, the use of a structure composed of $MoS_2$, $WS_2$, and Si in the field of photoelectricity, particularly in terms of optical absorptivity, has been scarcely investigated.

This paper investigates the transmission properties of various structures, including Si, $MoS_2$/Si, and $WS_2/MoS_2$/Si, under normal incidence in a broadband range. The thicknesses of $WS_2$, $MoS_2$, and Si were 30 nm, 30 nm, and 1 μm, respectively. The refractive indices of the materials were obtained from previously published literature [14-16].

## 2. Theory

When light travels through a medium with varying refractive index, such as a multilayer structure, it undergoes reflections and transmissions. The theory behind these phenomena has been extensively discussed in relevant papers [16]. The light source used in this study is a plane wave with a wavelength range of 0.3 μm to 2 μm. According to Maxwell's equations, the absorptivity (A) can be calculated using the formula A(λ)=1-R(λ)-T(λ), where R(λ) and T(λ) represent reflectivity and transmissivity, respectively, and λ denotes the wavelength. The expressions for R(λ) and T(λ) in multi-layer films have been derived and can be found in series formulae, such as formulas (1), (2), (3) and (4) [16], specifically for three films placed in air. These simplified formulas can also be applied to monolayer and bilayer films.

$$\begin{pmatrix} a & b \\ c & d \end{pmatrix} = \begin{pmatrix} 1 & r_1 \\ r_1 & 1 \end{pmatrix} \begin{pmatrix} e^{i\delta_1} & r_2 e^{i\delta_1} \\ r_2 e^{-i\delta_1} & e^{-i\delta_1} \end{pmatrix} \begin{pmatrix} e^{i\delta_2} & r_3 e^{i\delta_2} \\ r_3 e^{-i\delta_2} & e^{-i\delta_2} \end{pmatrix} \begin{pmatrix} e^{i\delta_3} & r_4 e^{i\delta_3} \\ r_4 e^{-i\delta_3} & e^{-i\delta_3} \end{pmatrix} \tag{1}$$

$$R = \frac{cc^*}{aa^*} \tag{2}$$

$$T = \frac{\left(t_1 t_2 t_3 t_4\right)\left(t_1^* t_2^* t_3^* t_4^*\right)}{aa^*} \tag{3}$$

$$\delta_m = \frac{2\pi}{\lambda} n_m d_m \cos\phi_m \tag{4}$$

where in the formula(1) the letter "e" is a constant, representing the exponential function. The "i" in the upper right corner of formula (1) represents the imaginary unit " i". "$r_1$, $r_2$, $r_3$, $r_4$" represent the reflection coefficients of each layer interface. In the formula (2), "a" and "c" represent the corresponding elements in the coefficient matrix, "a*" and "c*" represent their complex conjugate values. In the formula (3), "$t_1$, $t_2$, $t_3$, $t_4$" represent the transmittance coefficients of each layer interface, and the refractive index of each layer medium is a complex refractive index, so they are complex numbers. "$t_1$*, $t_2$*, $t_3$*, $t_4$*" represent the complex conjugate values of the transmittance coefficients of each layer interface. In the formula (4), "λ" represents the wavelength of light waves. "$n_m$" represents the refractive index of the medium, "$d_m$" represents the thickness of the medium, "$\delta_m$" represents the phase change of the light passing through each layer of the film, "$\varphi_m$" represents the angle of incidence of the light, and the subscript "m" indicates the serial number of each layer of the medium.

## 3. Method

The study on the reflection and transmission of Si, $MoS_2$/Si, and $WS_2$/$MoS_2$/Si is crucial for enhancing the performance of photodetector devices. The film thickness of each structure has been fixed accordingly, with Si serving as the bottom layer. The light beam is incident vertically for illumination. To simulate the optical transmission characteristics of these structures, we have utilized Meep, a free and open-source software package originally developed by MIT [17]. In Meep, the perfectly matched layer (PML) approach to implementing absorbing boundary conditions in FDTD simulation was originally proposed in the paper [18]. The approach involves surrounding the computational cell with a medium that in theory absorbs without any reflection electromagnetic waves at all frequencies and angles of incidence. The original PML formulation involved "splitting" Maxwell's equations into two sets of equations in the absorbing layers, appropriately defined.

The boundaries are defined at three coordinates namely x, y and z [19]. The unit cell boundary condition is applied at the x and y directions and open (add space) boundary condition is applied at the z direction. Defined boundaries with axis are shown in Fig. 1.

Meep allows us to assign the dielectric permittivity of materials using a Drude-Lorentz approximation. In Meep software simulation, we can approximate the material permittivity using one, two, or three Lorentz terms [20]:

$$\varepsilon(\omega) = \left(n + ik\right)^2 = \varepsilon_\infty + \sum_{p=1}^{3} \frac{\sigma_p \omega_p^2}{\omega_p^2 - \omega^2 - i\omega\gamma_p} \tag{5}$$

where n and k are the real and imaginary part of complex refractive index, respectively. $\varepsilon_\infty$ is high frequency dielectric constant, the meep unit of $\omega_p$ and $\gamma_p$ are μm-1, $\sigma_p$ is constant without unit. $\omega_p$ and $\gamma_p$ are user-specified constants. $\sigma_p$ is a user-specified function of position giving the strength of the $p$-th resonance.

Calculated by programming, being similar to the description in the papers [21, 22], the parameter values of the Drude-Lorentz formula (5) for Si, $MoS_2$, and $WS_2$ in the wavelength range of 0.3 μm to 2 μm are shown in table 1. as follows:

*Table 1. The parameter of the Drude-Lorentz formula for Si, $MoS_2$, and $WS_2$*

| Material | Si | $MoS_2$ | $WS_2$ |
|---|---|---|---|
| $\varepsilon_\infty$ | 1.1962 | 1.1016 | 2.3947 |
| $\sigma_1$ | 11.6857 | 0.0510 | 332.6179 |
| $\omega_1$ | 3.26 | 0.0419 | 0.0220 |
| $\gamma_1$ | 1.0157 | 2.3269e-14 | 2.0520e-7 |
| $\sigma_2$ | 1.2143 | 0.5171 | 2.0059 |
| $\omega_2$ | 0.1746 | 4.6424 | 2.4512 |
| $\gamma_2$ | 3.8223e+4 | 1.7775 | 0.6219 |
| $\sigma_3$ | 0.6324 | 46.8971 | 0.9275 |
| $\omega_3$ | 3.4366 | 0.0303 | 3.4787 |
| $\gamma_3$ | 0.1211 | 2.3244e-14 | 0.5228 |

The sandwich layered structures depicted in Fig.1 have been constructed using three different materials.

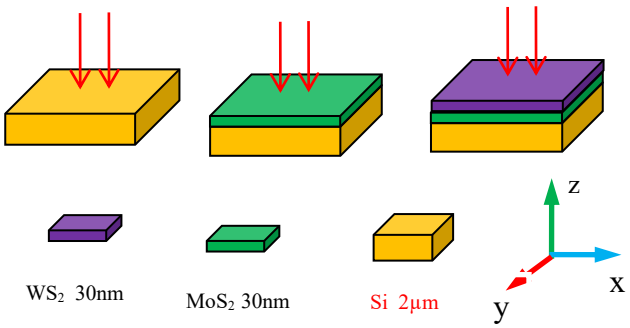


*Fig. 1. The structures composed of Si, $MoS_2$ and $WS_2$ (colour online)*

The Meep software was utilized to calculate the R(λ) and T(λ) values for the three structures. The absorptivity was determined using the formula A(λ) = 1 - R(λ) - T(λ).

## 4. Discussion

It is evident from Figs. 2 and 3 that there are significant variations in the absorptivities and transmissivities among the three structures.

In Fig. 2, the absorptivities of these structures increased with the addition of the material. Specifically, the absorptivity of the Si layer structure reached a maximum of 0.63 with a FWHM (Full Width at Half Maximum) of 0.8 μm within the wavelength range of 0.3 μm to 1.6 μm. The absorptivity of the $MoS_2$/Si bilayer structure had a similar value, around 0.65, within the wavelength range of 0.35 μm to 0.86 μm. However, the absorptivity of the $WS_2/MoS_2$/Si trilayer structure showed a significant increase and surpassed the absorptivity of the Si and $MoS_2$/Si structures across a broad spectrum. Examples of this situation are illustrated as follows: within the wavelength range of 0.3 μm to 0.43 μm, the FWHM is 0.04 μm with a maximum absorptivity of 0.9 at 0.34 μm. Within the wavelength range of 0.43 μm to 1.12 μm, the FWHM is 0.37 μm with a maximum absorptivity of 1.0 at 0.65 μm. With the addition of materials, the highest point experiences a blue shift, such as 0.75 μm in the Si layer, 0.7 μm in the $MoS_2$/Si layer film, and 0.65 μm and 0.34 μm in the $WS_2/MoS_2$/Si structure. When the wavelength exceeds 0.8 μm, the absorptivity in the Si and $MoS_2$/Si structures exhibits a similar behavior, linearly decreasing with a slope of approximately -0.33 until reaching 0.26. Similarly, when the wavelength exceeds 0.65 μm, the absorptivity in the $WS_2/MoS_2$/Si structure linearly decreases with a rake ratio of -0.53 until reaching 0.28. The absorptivity of $WS_2/MoS_2$/Si is at least 0.04 higher compared to the Si and $MoS_2$/Si structures. In general, the absorption characteristic of $WS_2/MoS_2$/Si is the best among the three structures.

The extinction coefficient of materials decides the absorptivities of the structures. The extinction coefficient of Si has a rapid descent from 5.3 to zero in the wavelength of 0.3 μm to 0.5 μm, and the value of $WS_2$ undergo the process of rising from 0.9 to 1.7 and then falling to zero in the visible wavelength range with the maximun of 1.7 in the wavelength of 0.4 μm. When the wavelenhtg is more than 0.8 μm, the extinction coefficient of Si and $WS_2$ are close to zero. At the same time, the extinction coefficient for $MoS_2$ is almost zero across the entire wavelength spectrum studied.

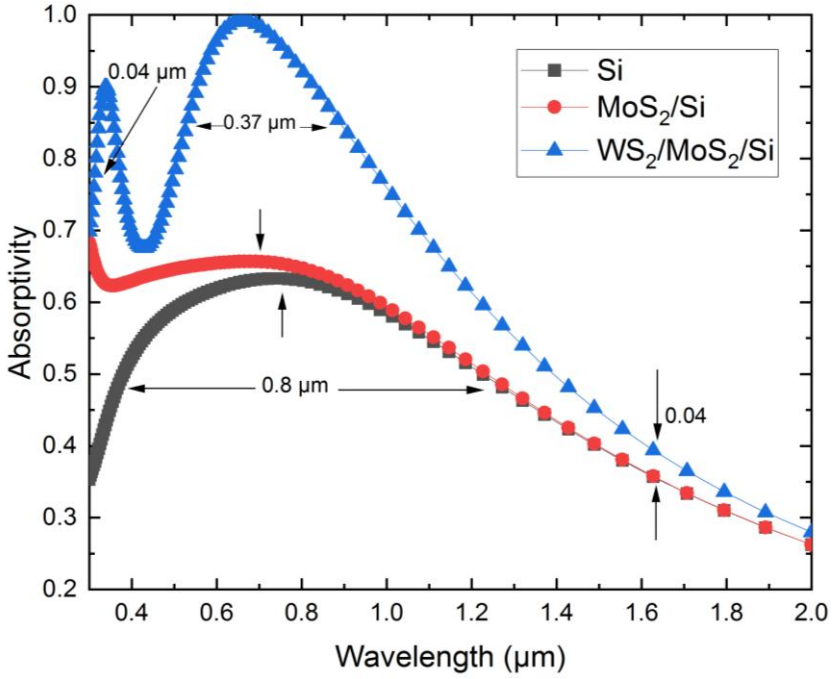


*Fig. 2. Absorptivities of structures (colour online)*

In Fig. 3, the transmissivity of these three structures is zero in the visible light range. However, from a wavelength of 0.8 μm to 2 μm, the transmissivity of Si and $MoS_2$/Si increases linearly with a slope of 0.34, reaching a value of 0.41. The curves for Si and $MoS_2$/Si overlap completely. Similarly, the transmissivity of $WS_2/MoS_2$/Si also increases linearly with a slope of 0.36, reaching a value of 0.43. Notably, the transmissivity of $WS_2/MoS_2$/Si is equal to or greater than the other two structures in both the visible light and near-infrared band. In the near-infrared band, the difference in transmissivity, known as the D-value, is approximately 0.03. This suggests that a thicker structure has a higher transmissivity in these conditions, which is a unique and interesting phenomenon.

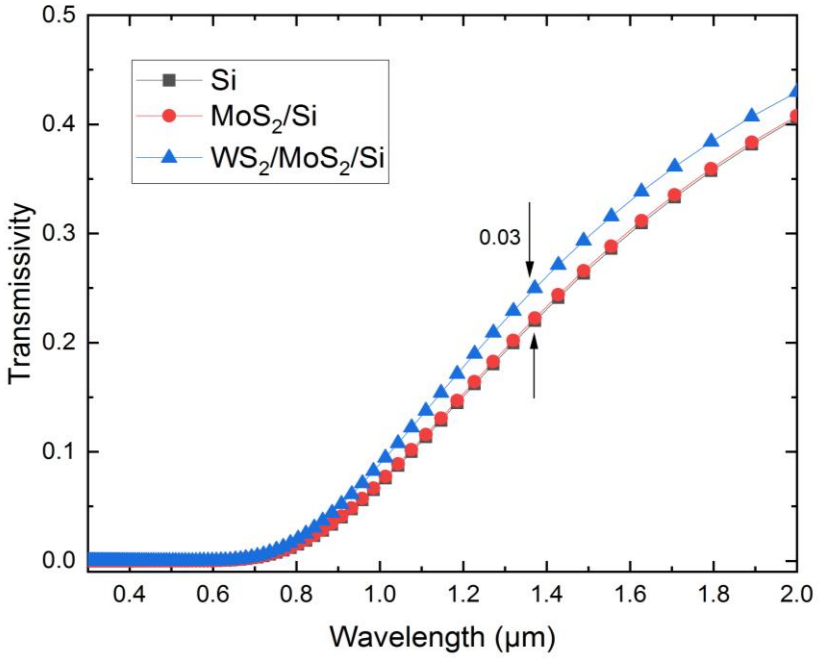


*Fig. 3. Transmissivities of structures (colour online)*

The absorptivity and transmissivity of $WS_2/MoS_2/Si$ show varying differences and have different addition when compared to Si and $MoS_2/Si$, as illustrated in Fig. 2 and Fig. 3. However, it is worth noting that the reflectivity of the structure is decreasing, as depicted in Fig. 4. The formula $A(\lambda)=1-R(\lambda)-T(\lambda)$ remains valid in this context and aligns with the principles of electromagnetic theory.

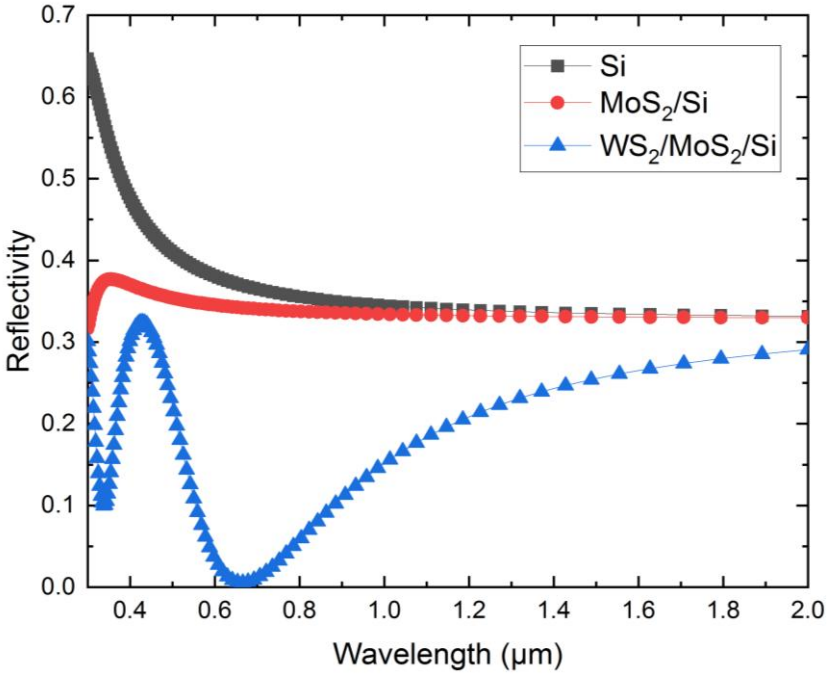


*Fig. 4. Reflectivities of structures (colour online)*

The phenomenon can be attributed to the unique characteristics of the refractive index of materials, as depicted in Fig. 5.

On one hand, Si exhibits tremendous anomalous dispersion, with a $dn/d\lambda$ value of 24.3 $\mu m^{-1}$, in the wavelength range from 0.3 μm to 0.36 μm. Similarly, $WS_2$ displays larger anomalous dispersion, with a $dn/d\lambda$ value of 10.5 $\mu m^{-1}$, in the wavelength range from 0.34 μm to 0.45 μm. However, both materials exhibit normal dispersion in other wavelength ranges. In the near-infrared

band, the real part of the refractive index for both Si and $WS_2$ remains relatively unchanged, with Si having a value close to 3.5 and $WS_2$ having a value around 2.3. $MoS_2$ exhibits normal dispersion in the visible light and near-infrared band, with a constant real part of the refractive index equal to 1.25.

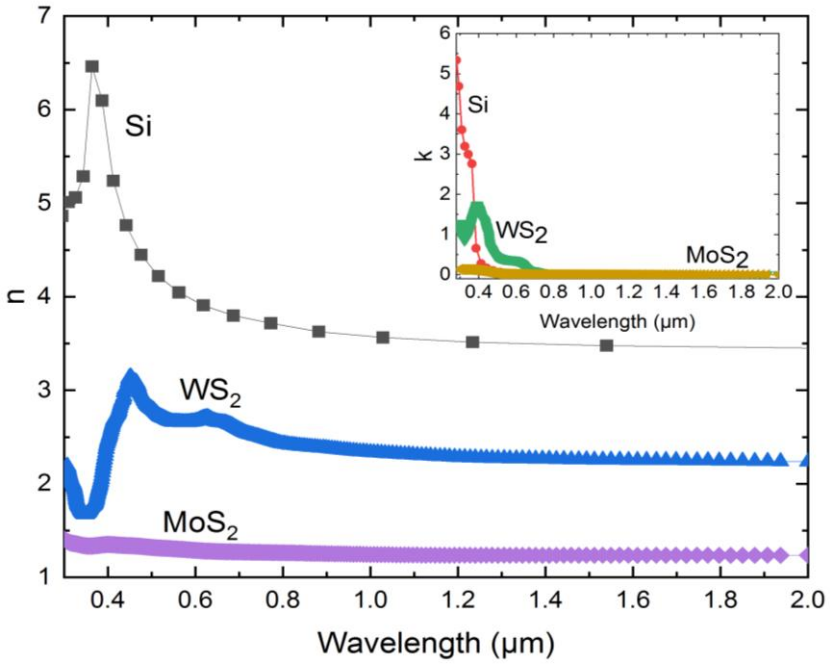


*Fig. 5. The complex refractive indexes of Si, WS2 and MoS2 (n, k denote the real and imaginary part, respectively) (colour online)*

On the other hand, the extinction coefficient of Si and $WS_2$ undergo significant changes in the visible wavelength range. For Si, there is a steep decrease in gradient with $dk/d\lambda = -41.9\ \mu m^{-1}$ for wavelengths less than 0.4 μm, followed by a near-zero gradient with wavelengths greater than 0.4 μm. In comparison, $WS_2$ exhibits an even more pronounced gradient with $dk/d\lambda = -21\ \mu m^{-1}$ between 0.33 μm and 0.4 μm, and a much higher gradient of $dk/d\lambda = 5.47\ \mu m^{-1}$ within the 0.4 μm to 0.7 μm wavelength range. In all other wavelengths, the extinction coefficient for Si and $WS_2$ remains close to zero. Interestingly, the extinction coefficient for $MoS_2$ is consistently negligible across the entire wavelength spectrum.

## 5. Conclusion

The $WS_2/MoS_2/Si$ structure significantly enhances absorption characteristics across a wide band, particularly in the visible light range. It exhibits improved absorptivity and expanded wavelength range compared to alternative structures. This makes it highly valuable for the development of photoelectric devices like photodetectors and solar cells.

### Acknowledgements

The project received support from the Project of Science and Technology of Henan Province in China (NO. 242102210172). Additionally, it was partially funded by the Cultivation Fund of the Key Scientific and Technical Innovation Project, Ministry of Education of China, through Grant 708038, and Henan Natural Science Foundation Project (NO. 232300420101).

### References

[1] Md. Khan Sobayel Bin Rafiq, N. Amin, Hamad F. Alharbi, Monis Luqman, Afida Ayob, Yahya S. Alharthi, Nabeel H. Alharthi, Badariah Bais, Md. Akhtaruzzaman, Sci. Rep. **10**(1), 771 (2020).
[2] G. Rudren, Q. Zhang, ACS Nano **8**(5), 4074 (2014).
[3] L. Dal Negro, M. Cazzanelli, L. Paves, S. Ossicini, D. Pacifici, G. Franzo, F. Priolo, F. Iacona, Appl. Phys. Lett. **82**(26), 4636 (2003).
[4] Olivia Pulci, Elena Degoli, Federico Iori, Margherita Marsili, Maurizia Palummo, Rodolfo Del Sole, Stefano Ossicini, Superlattice Microst. **47**(1), 178 (2010).
[5] L. Pavesi, L. Dal Negro, C. Mazzoleni, G. Franzo, F. Priolo, Nature **408**, 440 (2000).
[6] Mengyuan Ye, Chunlei Sun, Yu Yu, Yunhong Ding, Xinliang Zhang, Nanophotonics **10**(4), 1265 (2021).
[7] Y. Jiandong, Y. Guowei, Nanoscale **12**(2), 454 (2020).
[8] Rohit Sharma, Radhapiyari Laishram, Bipin Kumar Gupta, Ritu Srivastva,

Om Prakash Sinha, Advances in Natural Sciences: Nanoscience and Nanotechnology **13**(2), 23001 (2022).
[9] Lin Long, Shaohong Cai, Mingsen Deng, Mater. Res. Bull. **174**, 112732 (2024).
[10] Avneesh Kumar, Ajeet Gupta, Arun Kumar, Surbhi, Himanshu Sharma, Arvind Kumar, Mudit P. Srivastava, Devendra Kumar Rana, J. Sol-Gel Sci. Techn. **114**, 799 (2025).
[11] Oriol Lopez-Sanchez, Dominik Lembke, Metin Kayci, Aleksandra Radenovic, Andras Kis, Nature Nanotechnology **8**(7), 497 (2013).
[12] Chen Yichuan, S. Mengtao. Nanoscale **13**(11), 5594 (2021).
[13] Chunxiao Cong, Jingzhi Shang, Yanlong Wang, Ting Yu, Adv. Opt. Mater. **6**(1), 1700767 (2018).
[14] Li-Ping Feng, Han-Qing Sun, Ao Li, Jie Su, Yan Zhang, Zheng-Tang Liu, Mater. Chem. Phys. **209**, 146 (2018).
[15] Qing Luan, Chuan-Lu Yang, Mei-Shan Wang, Xiao-Guang Ma, Chinese J. Phys. **55**, 1930 (2017).
[16] O. S. Heavens, Optical properties of Thin Solid Films[M]. London: Butterworths Scientific Publications (1955).
[17] Ardavan F. Oskooi, David Roundy, Mihai Ibanescu, Peter Bermel, J. D. Joannopoulos, Steven G. Johnson, Comput. Phys. Commun. **181**(3), 687 (2010).
[18] Jean Pierre Berenger, Computational Physics **114**, 185 (1994).
[19] K. Vigneshwaran, R. Samson Daniel, J. Optoelectron. Adv. M. **27**(1-2), 1 (2025).
[20] Alexei Deinega, Ilya Valuev, Boris Potapkin, Yurii Lozovik, Journal of the Optical Society of America A **28**(5), 770 (2011).
[21] Jian Fei Liao, J. Optoelectron. Adv. M. **26**(5-6), 199 (2024).
[22] Y. Pan, J. Optoelectron. Adv. M. **26**(3-4), 91 (2024).

*Corresponding author: goodxinan@126.com